Artificial Neural Networks for Material Identification, Mineralogy and Analytical Geochemistry Based on Laser-Induced Breakdown Spectroscopy

Alexander Koujelev and Siu-Lung Lui
Canadian Space Agency[1]
Canada

1. Introduction

Artificial Neural Networks (ANN) are used nowadays in a broad range of areas such as pattern recognition, finances, data mining, battle scene analysis, process control, robotics, etc. Application of ANN in the field of spectroscopy has generated a long-standing interest of scientists, engineers and application specialists. The ANN' capability of producing fast, reliable and accurate spectral data processing has become, in many cases, a bridging mechanism between science and application. A particular example of how ANN can transform plasma emission spectroscopy, that is quit challenging to model, into a turnkey ready to use device is described in this Chapter.

Laser-Induced Breakdown Spectroscopy (LIBS) is a material-composition analytical technique gaining increased interest last decade in various application fields, such as geology, metallurgy, pharmaceutical, bio-medical, environmental, industrial process control and others (Cremer & Radziemski, 2006; Miziolek et al., 2006). It is in essence a spectroscopic analysis of light emitted by the hot plasma created on a sample by the laser-induced breakdown. LIBS offers numerous advantages as compared to the standard elemental analysis techniques (X-ray fluorescence or X-ray diffraction spectroscopy, inductively coupled plasma spectroscopy, etc.), such as: capability of remote analysis in the field, compact instrumentation, detection of all elements and high spatial resolution. Such features as minimum or no sample preparation requirement and dust mitigation using "cleaning" laser shots are especially important for field geology and remotely operated rover-based instruments.

As result, LIBS instruments have been selected as payloads for the 2011 Mars Science Laboratory mission led by the National Aeronautics and Space Administration (Lanza et al., 2010) and the ExoMars mission on Mars planned for 2018 and led by European Space Agency (Escudero-Sanz et al., 2008).

Despite of the advantages, the main challenge is still the retrieval of accurate information from measured spectra. LIBS spectral signals, composed mostly of narrow emission lines, are complex nonlinear functions of concentrations of measured constituents and instrument

---

[1] *© Government of Canada 2010*

parameters. The most important contributors to this nonlinearity are spectral overlapping, self-absorption, and the so-called matrix effects. These effects are caused by chemical properties and morphological features of the sample matrix that can change the intensity of the emitted lines (Eppler et al., 1996; Harmon et al., 2006). In addition, the ambience such as pressure, temperature and gas type can vary the heat loss and confinement effect in LIBS that results in a change of spectra (Iida, 1990; Lui & Cheung, 2003). All this leads to large errors in concentration measurements of minor or trace elements performed in different materials. This became a serious impeding factor for using full advantages of LIBS in analytical geochemistry in either field geology or planetary exploration.

Common quantitative spectral data processing algorithms, based on calibration curve method have been successfully applied in some cases (St-Onge et al., 2002; Cho et al., 2001), but they are limited to application in one class of material and require *a priory* knowledge about the tested sample. An alternative method, called calibration-free method, relies on plasma model to calculate plasma temperature using several spectral lines. It shows encouraging results, however also subject to a number of limitations (Ciucci et al., 1999; Aguilera et al., 2009).

Classification & identification techniques are also used in conjunction with LIBS to define material identity and even composition. In relatively simple cases classification and identification of samples can be achieved by evaluating the line ratios or the patterns of a LIBS spectrum (Mönch et al., 1997; Samek et al., 2001; Sattmann et al., 1998). More sophisticated classification methods such as, principle components analysis (PCA), soft independent modeling of class analogy (SIMCA) and partial least-squares discriminant analysis (PLS-DA), have been studied and produced very promising results (Sirven et al., 2007; Clegg et al., 2009). However, the above techniques being based on linear processing have difficulty to take into account nonlinear effects.

ANN data processing offers to address the above challenges as having the potential to solve nonlinear problems (Gurney, 1997; Haykin, 1999). The capabilities of ANN in this area have started to be explored recently almost simultaneously by few groups. Inakollu (Inakollu et al., 2009) used ANN to predict the element concentrations in aluminium alloys from its LIBS spectrum. Ferreira (Ferreira et al., 2008) selected a set of wavelengths through the "wrapper" algorithm and then determined the concentration of copper in soil samples by ANN. Sattmann (Sattmann et al., 1998) discriminated PVC from other polymers with the distinct chlorine 725.66 nm line. Ramil (Ramil et al., 2008) classified the LIBS spectra of 36 archaeological ceramics into three groups by ANN. The possibility of using ANN to predict composition in natural rocks explored in our earlier works by Motto-Ros (Motto-Ros et al., 2008) and Koujelev (Koujelev et al., 2009). We also demonstrated the capability of mineral and rock sample identification with LIBS combined with ANN (Koujelev et al., 2010). The potential of ANN to analyse LIBS spectra has been proven in these studies.

It is important to note that performing LIBS on geological material: minerals, rocks, and soils, is especially challenging. These materials can vary from silica-based basalt rock to iron-rich hematite mineral. They exhibit serious matrix effect thus the conventional calibration curve method will not be applicable for quantitative study (retrieval of composition). Most importantly, without prior knowing the matrix identity, choosing an appropriate calibration curve is impossible. Identification, or qualitative analysis, is also difficult to achieve since there are over few thousand types of minerals so learning all their spectra seems impractical. In fact, applying LIBS on rocks, soils or minerals have been reported in several studies. Menut (Menut et al., 2006) demonstrated the potential of probing europium in argillaceous rocks preconditioned in europium solution. Sharma

(Sharma et al., 2007) combined LIBS with Raman spectroscopy to evaluate mineral rocks. Bousquet (Bousquet et al., 2007) measured the chromium concentration in 22 soil samples doped with chromium. Calibration curve was obtained from the five kaolinite soil samples only. They also performed classification by principal components analyses (Sirven et al., 2006). Belkov (Belkov et al., 2009) showed the possibility of measuring the carbon content in 11 soil samples. The calibration curve was fit by an exponential function within 2% to 8% range. Gaft (Gaft et al., 2009) evaluated the performance of LIBS in sulphur analyses of minerals, alloys, and coal mixtures. Two calibration curves were established for two sets of coal mixtures. From these examples one can observe that the application of LIBS on geological analysis is mainly demonstrative and descriptive. Samples were artificially doped and the calibration curves were conditional, either limited by sample type or concentration range. In term of quantitative and qualitative aspects, the application on geological samples still remains challenging to the LIBS community.

This chapter presents a review of our earlier work as well as some new results. The focus is made on how we apply and optimise ANN in a particular spectroscopy application. The chapter is structured in the following way. After the introduction, the section describing the principles of LIBS will be presented so, that the particularities of the LIBS data are introduced. Some pre-processing techniques are presented in the LIBS section. The next, section is devoted to different ANN architectures used for particular types of data analysis and the targeted applications. The first sub-section describes material identification analysis, the second sub-section describes quantitative mineralogy analysis, and the third sub-section describes quantitative elemental analysis. Conclusions and future works are discussed in the last section of the chapter.

2. LIBS technique

Before we discuss different ANN spectral processing schemes, it is important to define the experimental settings where the raw spectra are obtained. It is also very important to address what types of materials are studied and what pre-processing routines are applied before the data are inputted to the network.

A typical LIBS system includes a laser, optical elements to focus laser beam and to collect plasma emission, and a spectrometer (Fig. 1). In our studies, the laser source is a Q-switch Nd:YAG laser (Spectra Physics, LPY150, 1064nm, 7 ns) operating at 1 Hz repetition rate with pulse energy of 20 mJ. The pulse energy is monitored by Joule-meter and adjusted by a $\lambda/2$ plate and a polariser. The beam is focused to a 50 µm spot to ablate the sample. The plasma emission is collected and delivered to the Ocean Optics LIBS 2000 spectrometer (200 – 970 nm, 0.1 mm resolution) through an optical fibre. In the majority of our experiments, the distance between the sample and the collection optics was 10 cm. The delays between instruments are controlled by a pulse delay generator (BNC 575). The spectra are recorded and analysed with a computer and dedicated software. It worth noting that these parameters are typical for a low-power LIBS system that may be used on a remote platform, such as planetary rover, or as a hand-held instrument in the field conditions.

Different types of geological materials are studied in our experiments. The samples of standard geological materials, mostly silicates in our cases, are supplied in form of powder with certified elemental composition by the Brammer Standard Company Inc. They are pressed into tablets for easy handling and sampling. Another set of natural rock and mineral samples is obtained from Miners Inc (part number: K4009). For these samples, only major

composition elements were known based on the type of mineral. Powder-based samples are used to train, validate and test the composition retrieval algorithm, while the natural rocks and minerals are used only to test the mineral identification capability.
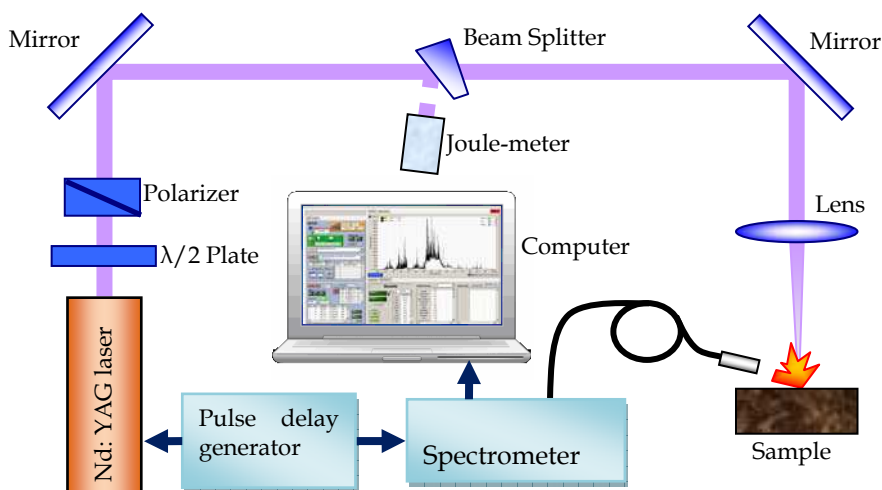

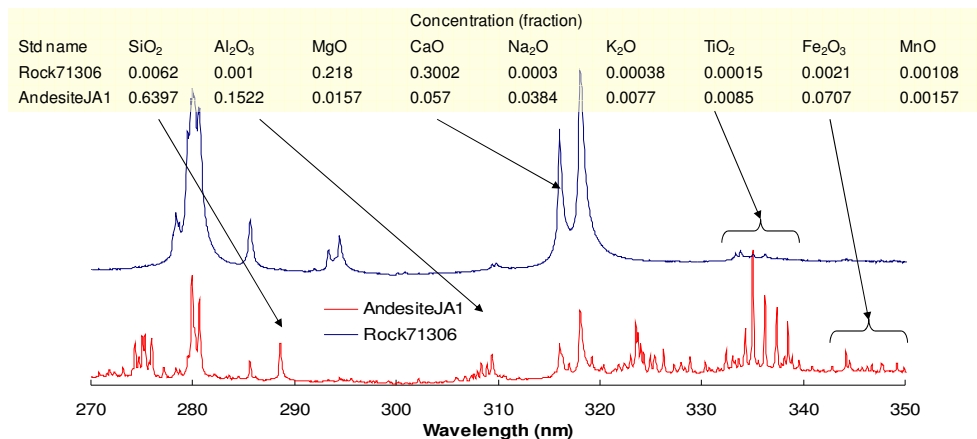Fig. 1. Experimental configuration of a LIBS system.

Std name	SiO$_2$	Al$_2$O$_3$	MgO	CaO	Na$_2$O	K$_2$O	TiO$_2$	Fe$_2$O$_3$	MnO
Rock71306	0.0062	0.001	0.218	0.3002	0.0003	0.00038	0.00015	0.0021	0.00108
AndesiteJA1	0.6397	0.1522	0.0157	0.057	0.0384	0.0077	0.0085	0.0707	0.00157

Fig. 2. Examples of LIBS spectra for materials with different composition.

Let us consider few examples of raw LIBS spectra. Spectral signatures of a carbonate rock (Rock 71306) and an andesite (JA1) are shown in Fig. 2. Due to large difference in compositions of these two materials, their discrimination can be easily arranged. Here, a monitoring of intensities of several key atomic lines (Si, Al, Ca, Ti and Fe in this case) can be employed. Therefore, identification or classification of types of minerals with a strong difference in composition can be easily achieved using simple logic algorithms. In this case, we rather care about the presence of specific spectral lines than the exact measurement of their intensity and correspondence to elemental concentration.

The situation however, can be much more complex when one deals with identification of materials with high degree of similarity, or with retrieval of compositional data (quantitative analysis). Such an example is presented in Fig. 3. Here the strategy for these two applications may diverge. Such, that for material identification the spectral lines showing the largest deviations between materials (Mg in this example) should be used. However, for quantitative analysis it is rather useful to select the spectral lines that exhibit near-linear correspondence of the intensity and the element concentration (Ti 330 nm – 340 nm lines in this example). This is why the material identification and quantitative analysis that will be discussed in the following sections rely on different spectral line selection.

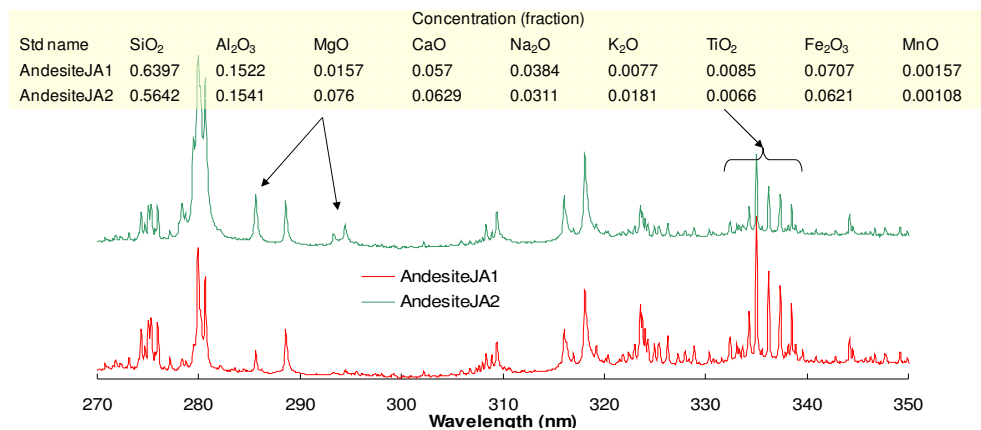|	Concentration (fraction)								
Std name	SiO_2	Al_2O_3	MgO	CaO	Na_2O	K_2O	TiO_2	Fe_2O_3	MnO
AndesiteJA1	0.6397	0.1522	0.0157	0.057	0.0384	0.0077	0.0085	0.0707	0.00157
AndesiteJA2	0.5642	0.1541	0.076	0.0629	0.0311	0.0181	0.0066	0.0621	0.00108

Fig. 3. Examples of LIBS spectra for materials with similar composition.

Once LIBS spectra are acquired from the sample of interest, several pre-processing steps are performed. Pre-processing techniques are very important for proper conditioning of the data before feeding them to the network and account for about 50 % of success of the data processing algorithm. The following major steps in data conditioning are employed before the spectral data are inputted to the ANN.

a. Averaging of LIBS spectra. Usually, averaging of up to a hundred of spectral samples (laser shots) may be used to increase signal to noise ratio. The averaging factor depends on experimental conditions and the desired sensitivity.

b. Background subtraction. The background is defined as a smooth part of the spectrum caused by several factors, such as, dark current, continuum plasma emission, stray light, etc. It can be cancelled out by use of polynomial fit.

c. Selection of spectral lines for the ANN processing. Each application requires its own set of selected spectral lines for the processing. This will be discussed in greater details in the following sections.

d. Calculation of normalised spectral line intensities. In order to account for variations in laser pulse energy, sample surface and other experimental conditions the internal normalization is employed. In our studies, we normalize the spectra on the intensity of O 777 nm line. This is the most convenient element for normalization since all our samples contain oxygen and there is always a contribution of atmospheric oxygen in the spectra in normal ambient conditions. The line intensities are calculated by integrating the corresponding spectral outputs within the full width half-maximum (FWHM) linewidth.

After this pre-processing, the amount of data is greatly reduced to the number of selected normalized spectral line intensities, which are submitted to the ANN.

3. ANN processing of LIBS data

The ANN usually used by researchers to process LIBS data and reported in our earlier works is a conventional three-layer structure, input, hidden, and output, built up by neurons as shown in (Fig. 4). Each neuron is governed by the log-sigmoid function. The first input layer receives LIBS intensities at certain spectral lines, where one neuron normally corresponds to one line.

A typical broadband spectrometer has more than a thousand channels. Inputting to the network the whole spectrum increases the network complexity and computation time. Our attempts to use the full spectrum as an input to ANN were not successful. As a result, we selected certain elemental lines as reference lines to be an input to ANN. General criteria for the line selection are the following: good signal to noise ratio (SNR); minimal overlapping with other lines; minimal self-absorption; and no saturation of the spectrometer channel.
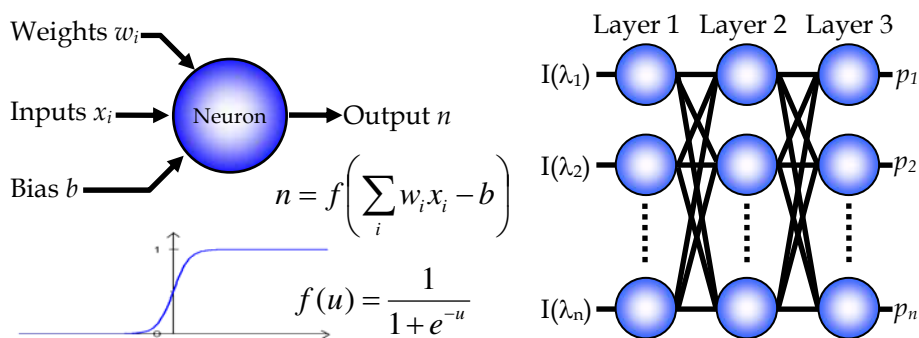

Fig. 4. Basic structure of an artificial neural network.

These criteria eliminate many lines which are commonly used by other spectroscopic techniques. For example, the Na 589 nm doublet saturates the spectrometer easily, thus is not selected. The C 247.9 nm can be confused with Fe 248.3 nm, therefore is avoided. At the same time, the relatively weak Mg 881 nm line is preferred to 285 nm line since it is located in a region with less interference from other lines. In addition to these general rules, some specific requirements for line selection imposed by particular applications are discussed in the following sections.

The number of neurons in the hidden layer is adjusted for faster processing and more accurate prediction. Each neuron at the output layer is associated either to a learnt material (identification analysis) or an element which concentration is measured (quantitative analysis). The output neurons return a value between 0 and 1 which represents either the confidence level (CL) in identification or a fraction of elemental composition in quantitative processing.

The weights and biases are optimized through the feed-forward back-propagation algorithm during the learning or training phase. To perform ANN learning we use a

Artificial Neural Networks for Material Identification, Mineralogy and
Analytical Geochemistry Based on Laser-Induced Breakdown Spectroscopy

97

training data set. Then to verify the accuracy of the ANN processing we use validation data set. Training and validation data sets are acquired from the same samples but at different locations (Fig. 5). In this particular example ten spectra collected at each location and averaged to produce one input spectrum per location. Five cleaning laser shots are fired at each location before the data acquisition.
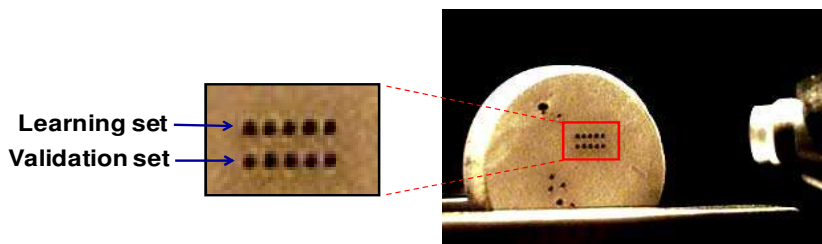
Fig. 5. Acquiring learning and validation spectra from a pressed tablet sample. The ten spots on the left are laser breakdown craters corresponding to the data sets. An emission collection lens is shown on the right in the picture.

3.1 Material identification

Material identification has been demonstrated recently with a conventional three-layer feed-forward ANN (Koujelev et al., 2010). High success rate of the identification algorithm has been demonstrated with using standard samples made of powders (Fig. 6). However, a need for improvements has been identified to ensure the identification is stable with given large variations of natural rocks in terms of surface condition, inhomogeneity and composition variations (Fig. 7). Indeed, the drop in identification success rate between validation set and the test set composed of natural minerals and rocks is from 87 % to 57 % (Fig. 6). Note, at the output layer, the predicted output of each neuron may be of any value between 0 (complete mismatch) and 1 (perfect match). The material is counted as identified when the ANN output shows CL above threshold of 70 % (green dashed line). If all outputs are below this threshold, the test result is regarded as unidentified. Additional, soft threshold is introduced at 45 % (orange dashed line) such that if the maximum CL falls between 45 % and 70 %, the sample is regarded as a similar class.

An improved design of ANN structure incorporating a sequential learning approach has been proposed and demonstrated (Lui & Koujelev, 2010). Here we review those improvements and provide a comparative analysis of the conventional and the constructive leaning network.

Achieving high efficiency in material identification, using LIBS requires a special attention to the selection of spectral lines used as input to the network. In addition to the above described considerations, we added an extra rational for the line selection. Lines with large variability in intensity between different materials, having pronounced matrix effects were preferred. In such a way we selected 139 lines corresponding to 139 input nodes of the ANN. The optimized number of neurons in the hidden layer was 140, and the number of output layer nodes was 41 corresponding to the number of materials used in the training phase.
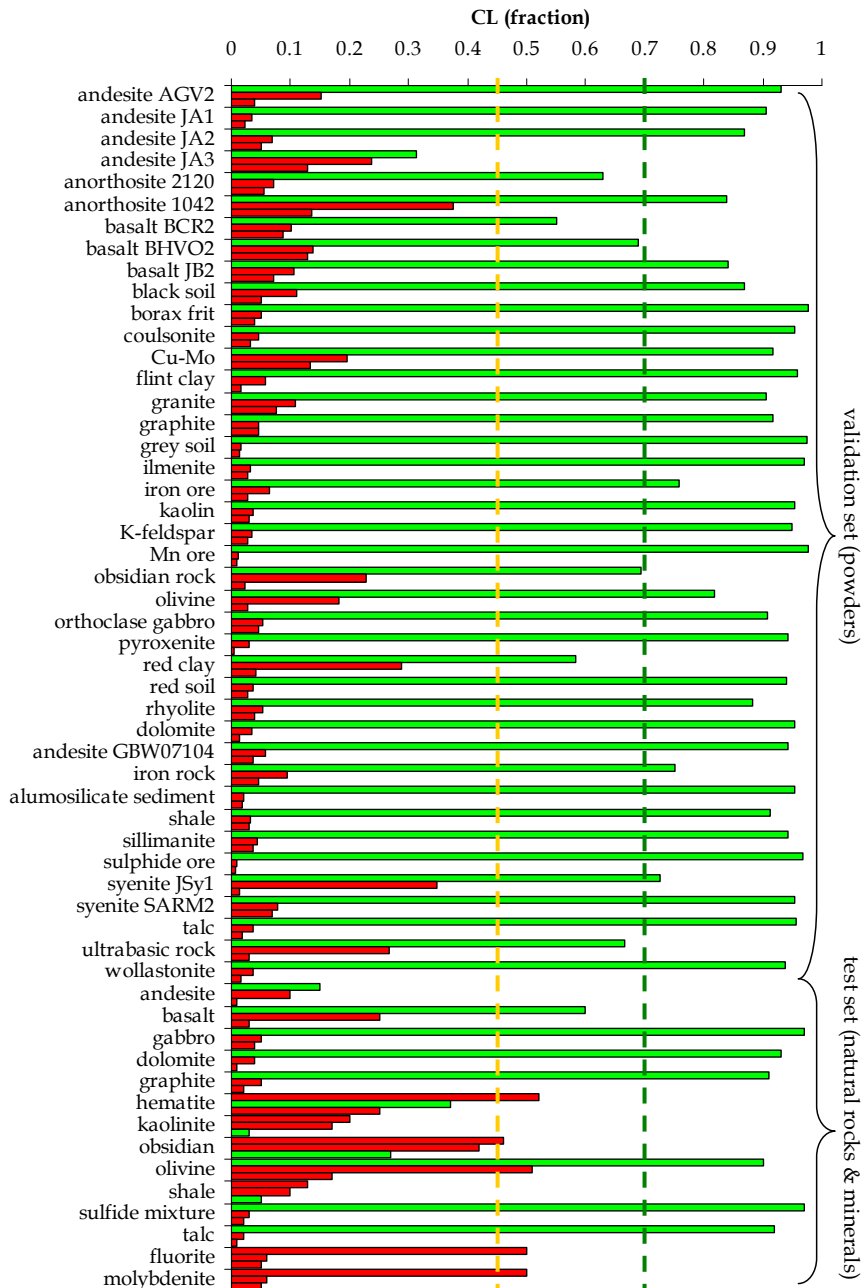
Fig. 6. Identification results for ANN with conventional training: powder tablets validation and natural rock & mineral test. Green colour corresponds to confidence levels for correct identification and red colour corresponds to mis-identification ANN outputs.
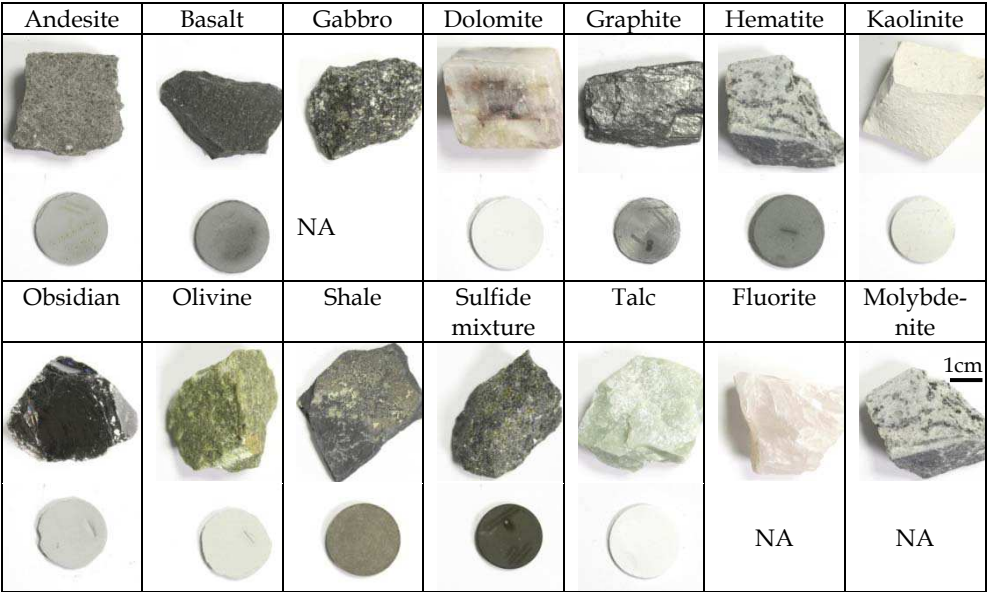
Andesite	Basalt	Gabbro	Dolomite	Graphite	Hematite	Kaolinite
		NA				

Obsidian	Olivine	Shale	Sulfide mixture	Talc	Fluorite	Molybde-nite
					NA	NA

Fig. 7. Natural rock & mineral samples and their powder tablets counterparts.

Randomly initialized weights & biases

1st training subset → 1st ANN training

Weights & biases from the 1st training

2nd training subset → 2nd ANN training

Weights & biases from the 2nd training

3rd training subset → 3rd ANN training

Weights & biases from the 3rd training

4th training subset → 4th ANN training

Weights & biases from the 4th training

5th training subset → 5th ANN training → **Trained ANN**

Fig. 8. Sequential training diagram.

When dealing with a conventional training the identification success rate drops rapidly if natural rock samples are subject to measurement on the ANN trained with powder made samples. This is, as we believe, due to overfitting of ANN. To avoid overfitting, the number of training cases must be sufficiently large, usually a few times more than the number of variables (i.e., weights and biases) in the network (Moody, 1992). If the network is trained

only by the average spectrum of each sample corresponding to 41 training cases, then the ANN is most likely to be overfitted. To improve the generalization of the network, the sequential training was adopted as an ANN learning technique (Kadirkamanathan et al., 1993; Rajasekaran et al., 2002 and 2006).

The early stopping also helps the performance by monitoring the error of the validation data after each back-propagation cycle during the training process. The training ends when the validation error starts to increase (Prechelt, 1998). In our LIBS data sets there are five averaged spectra per sample, each used in its own step of the training sequence. At each step, the ANN is trained by a subset of spectra with the early stopping criterion and the optimized weights and biases are transferred as the initial values to the second training with another subset. This procedure repeats until all subsets are used.

The algorithm implementation is illustrated in (Fig. 9). While the mean square error (MSE) decreases going through 5 consecutive steps (upper graph), the validation success rate grows up (bottom graph).
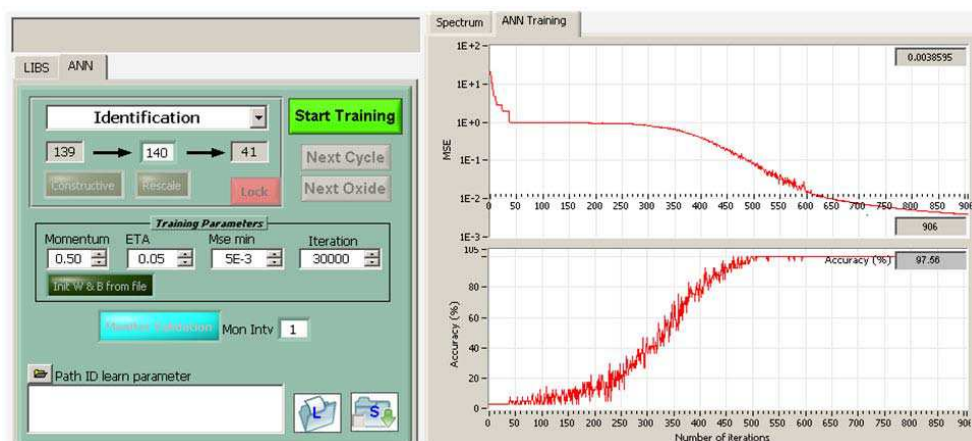
Fig. 9. Identification algorithm programmed in the LabView environment: the training phase.

Using a standard laptop computer the learning phase is usually completed in less than 20 minutes. Once the learning is complete, the identification can be performed in quasi real time. The LIBS-ANN algorithm and control interface is shown in (Fig. 10).

Identification can be performed on each single laser shot spectrum, on the averaged spectrum, or continuously. The acquired spectrum displayed is of the Ilmenite mineral sample in the given example. When the material is identified, the composition corresponding to this material is displayed. Note, that the identification algorithm does not calculate the composition based on the spectrum, but takes the tabular data from the training library. The direct measurement of material's composition is possible with quantitative ANN analysis.

In the event if the sample shows low CL for all ANN outputs it is treated as unknown. In such a case, more spectra may be acquired to clarify the material identity. If it is confirmed by several measurements that the sample is unknown to the network, it can be added to the

training library and the ANN can be re-trained with the updated dataset. Thus, for a remote
LIBS operation, this mode "learn as you go" adds frequently encountered spectra on the site
as the reference spectra. This mode offers a solution for precise identification without
dealing with too large database of reference materials spectra beforehand. The exact identity
or a terrestrial analogue (in case of a planetary exploration scenario) can be defined based on
more detailed quantitative analysis, possibly, in conjunction with data from other sensors.
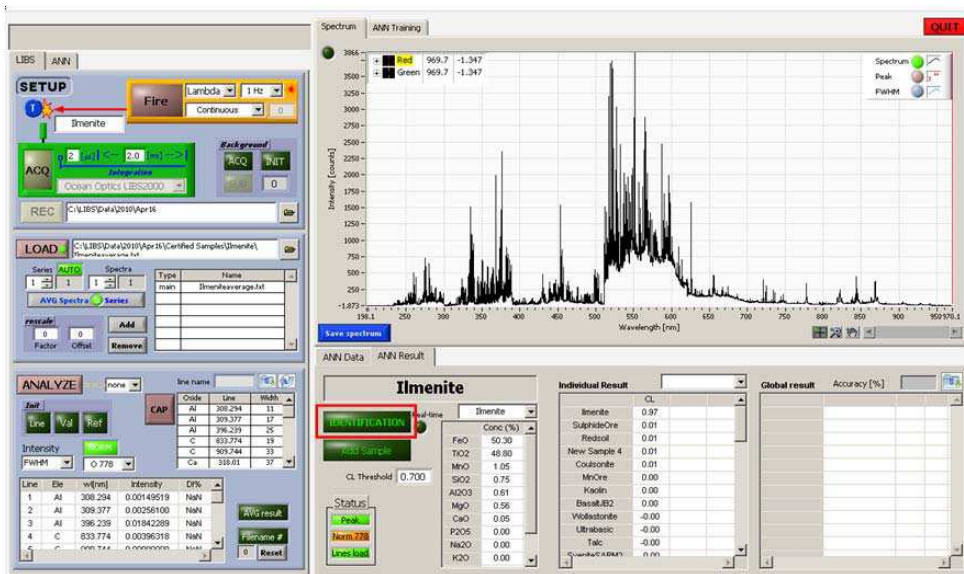
Fig. 10. Identification algorithm programmed in the LabView environment: how it works for
a test sample that has been identified. Upper-left section defines the hardware control
parameters. Bottom-left section defines the spectral analysis parameters (spectral lines).
Top-right part displays the acquired spectrum. Bottom-right section displays identification
results.

The results of validation and natural rock test identification are shown in (Fig 11) in the
form of averaged CL outputs. The CL values corresponding to mis-identification (red) are
lower than for the conventional training, especially for the part with natural rocks. All
identifications are correct in this case. The standard powder set includes similar powders of
andesite, anorthosite and basalt which are treated as different classes during the trainings.
Therefore, non-zero outputs may be obtained for their similar counterparts. The lower red
outputs in sequential training suggests it is more subtle to handle similar class. Note that
both training methods confuse andesite JA3, with other andesites. According to the certified
data, the concentrations of major oxides for JA3 always lie between those of other andesites.
As a result, there are no distinct spectral features to differentiate JA3 from other andesites.
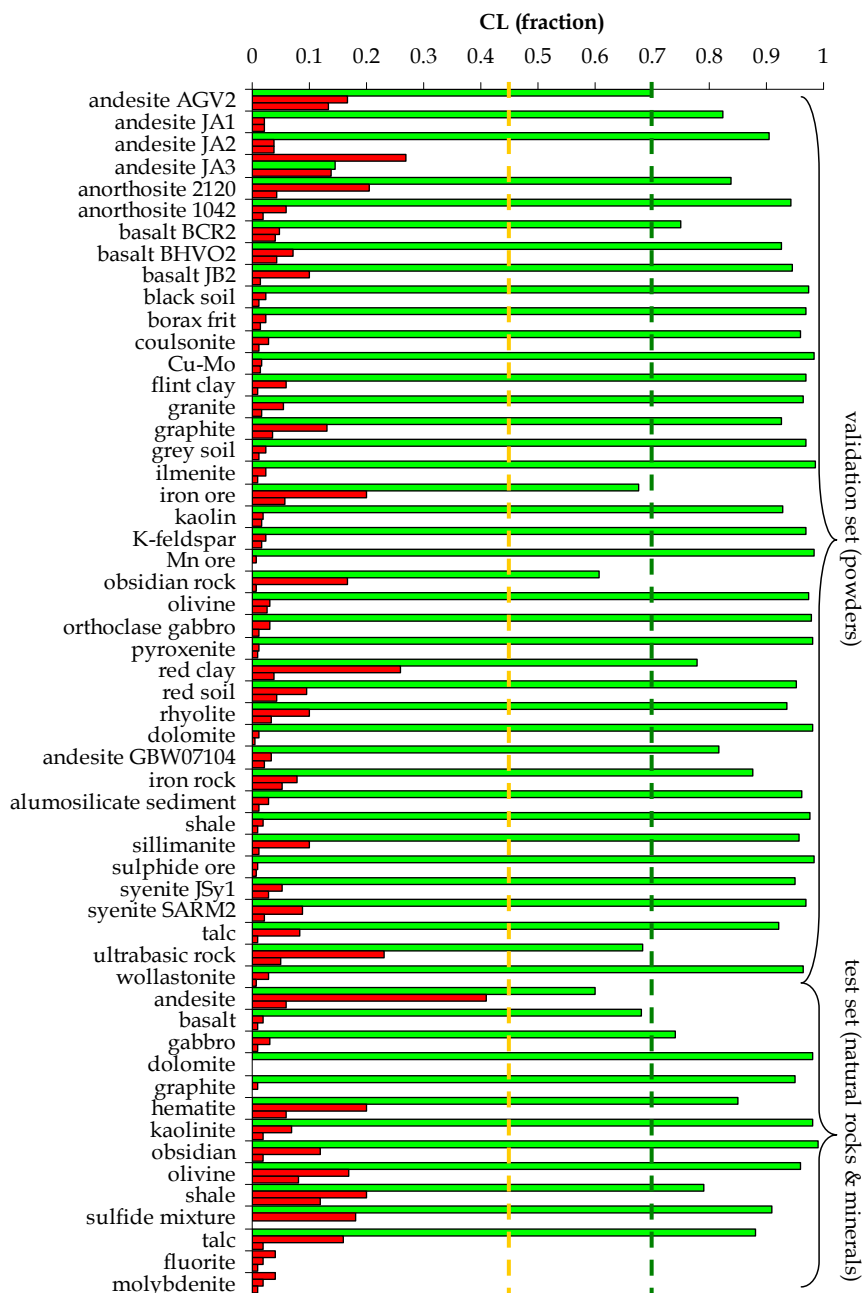Therefore, mis-identification in this particular case can be acceptable.

Fig. 11. Identification results for ANN with sequential training: powder tablets validation and natural rock & mineral test. Green colour corresponds to confidence levels for correct identification and red colour corresponds to mis-identification ANN outputs.

The last two samples, fluorite and molybdenite, are selected to evaluate the network's response to an unknown sample. The technique is capable of differentiating new samples. Certainly, if our certified samples included fluorite or molybdenite, the ANN would have been spotted these samples easily due to the distinct Mo and F emission lines.

The comparative of summary the results of the ANN with sequential training with those of another ANN trained by conventional method are shown in Table 1. Here, the conventional method is referred as a single training with one average spectrum for each sample. The prediction of the sequential LIBS-ANN improves with the increasing number of sequential trainings. After the 5th training, its performance surpasses that of the conventional LIBS-ANN. The rate of correct identification rises from 82.4% to 90.7%, while the incorrect identification rate drops from 2% to 0.5%. This is equivalent to only two false identifications out of 410 test spectra from the validation set. The rock identification shown is done on 50-averaged spectra. The correct identification rate for the sequential training method is 100%. In conventional training, it is only 57% with the rest results regarded as "undetermined". The outstanding performance of the sequential ANN shows a better generalization and robustness of the network.

| Material set | Training method | | Average rate (%) | | | |
| | | | Classified | | | |
			Correct	Misidentified	Success within classified samples	Unidentified
Validation set (powders)	Conventional		87.1	2.0	97.9	11.0
	Sequential training	After 1st	82.4	2.0	96.7	15.6
		After 3rd	88.5	1.7	97.5	9.8
		After 5th	90.7	0.5	99.5	8.8
Test set (natural rocks & minerals)[1]	Conventional		57.1	0	100	42.9
	Five level sequential training		100	0	100	0

Table 1. Validation and test result of the ANN trained by sequential and conventional methods. Average spectrum of a sample is used for testing.

3.2 Mineralogy analysis

Measuring presence of different minerals in natural rock mixtures is an important analysis that is commonly done in geological surveys. On one hand, LIBS relies on atomic spectral signatures directly indicating elemental composition of the material, therefore material crystalline structure does not appear to be present in the measurement. On the other hand, the information on the material physical and chemical parameters is present in the LIBS signal in a form of matrix effect. This, in fact, means that materials with the same elemental
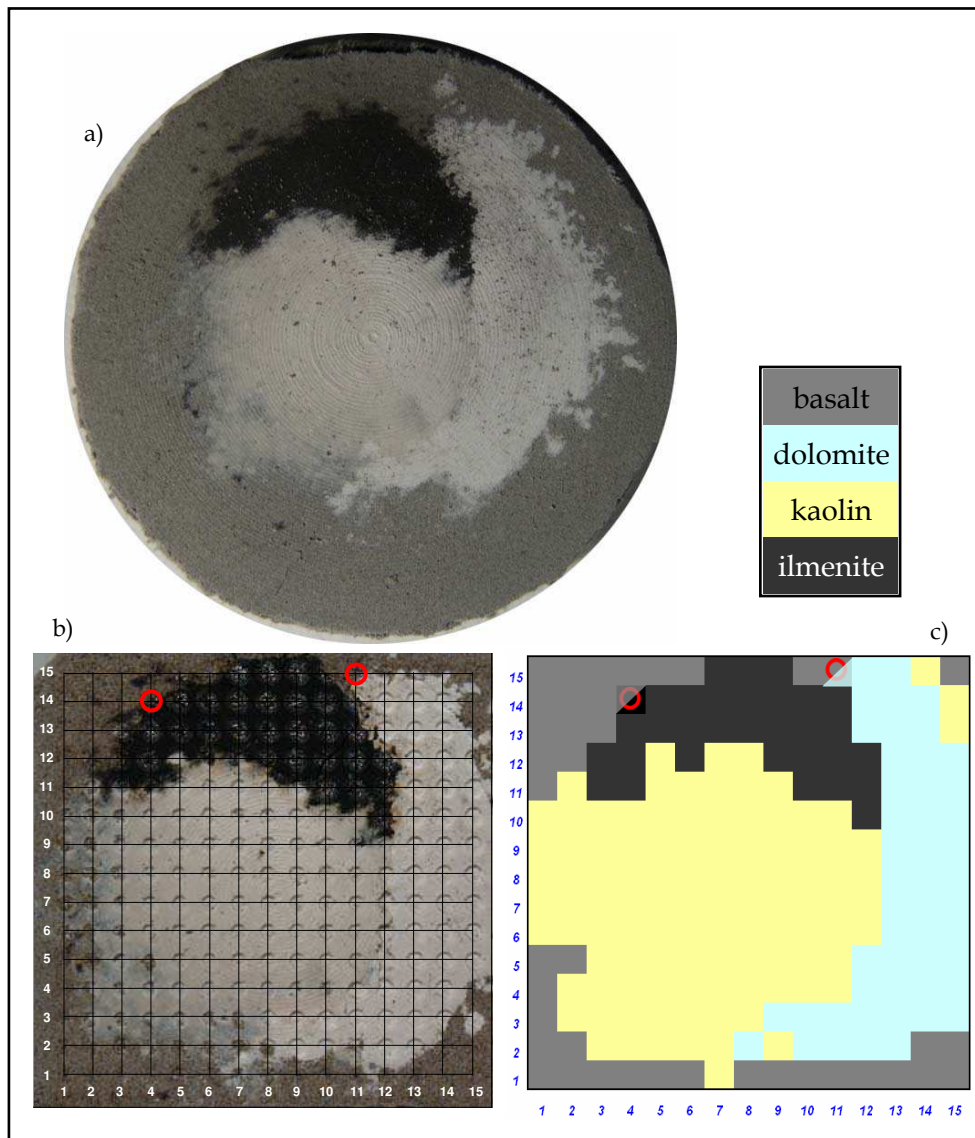
Fig. 12. Mineralogy analysis on the sample made of mixture of basalt, dolomite, kaolin and ilmenite. Red circles indicate unidentified prediction.

composition but different crystalline structure (or other physical or chemical properties) produce LIBS spectra with different ratios of spectral line intensities. Thus, mineralogy analysis can be done based on LIBS measurement where the ratios & intensities of the spectral lines are processed to deduce the identity of the mineral matrix.

One can implement this using the identification algorithm described in the previous section. The methodology relies on a series of measurement produced in different locations of the

rock, soil or mixture, where only one mineral type is identified in each location. Then, the quantitative mineralogy content in percents is generated for the sample based on the total result.

In this section, we describe a mineralogy analysis algorithm and tests that were performed in a particular low-signal condition. LIBS setup, described earlier, was used with a larger distance between the collection aperture and a sample. The distance was increased up to 50 cm thus resulting in 25 times smaller signal-to-noise ratio. This simulates realistic conditions of a field measurement. Since a lens of longer focal length was used, a larger crater was produced.

Because of low-signal condition, we adjusted ANN structure to produce result that is more reliable. First, the peak value is used in this case instead of FWHM-integrated value used earlier to represent the spectral line intensity. In a condition of weak lines, the FWHM value is difficult to define. Second, the intensities of several spectral lines per element were averaged to produce one input value to the ANN. Consequently, the ANN structure included 10 input nodes (first layer) corresponding to the following input elements: Al, Ca, Fe, K, Mg, Mn, Na, P, Si and Ti. The output layer contained 38 nodes corresponding to the number of mineral samples in the library. The hidden layer consisted of 40 neurons. The sequential training described above was used.

In order to test the performance of quantitative mineralogy, an artificial sample was made based on the mixture of certified powders. Four minerals such as, ilmenite, basalt, dolomite and kaolin, were placed in a pellet so that clusters with visible boundaries can be formed after pressing the tablet (Fig. 12a). The measurements were produced by a map of 15x15 locations with a spacing of 1 mm where LIBS spectra were taken (Fig. 12b). Ten measurement spectra were taken at each location. They are averaged and processed by ANN algorithm.

Figure 12c shows the resulting mineralogy surface map. Since the colours of mineral powders were different, one may easily compare the accuracy of the LIBS mineralogy mapping with the actual mineral content. The results of the scan are summarised in the Table 2. The achieved overall accuracy is 2.5 % that is an impressive result demonstrating the high potential of the technique.

Mineral	Basalt	Dolomite	Kaolin	Ilmenite
LIBS-ANN measurement, %	17.8	21.8	45.8	13.8
True value, %	22.2	18.2	46.9	12.7
Deviation, %	4.4	3.6	1.1	1.1
Average deviation, %	2.5			

Table 2. Test result of the LIBS-ANN mineralogy mapping.

It should be noted that the true data are calculated as percentages of the mineral parts present on the scanned surface. These percentages are not representative of the entire surface of the sample or volume content. This becomes an obvious observation if one

considers that the large non-scanned area at the edge of the sample is covered by basalt, while its abundance is small on the scanned area. Therefore, the selection of the scanning area becomes very important issue if the results are to be generalised on entire sample.

3.3 Quantitative material composition analysis

The mineralogy analysis based on identification ANN can be used to estimate material elemental composition. This estimation however may largely deviate from true values, because it is based on the assumption that each type of mineral (or reference material) has well defined elemental composition. In reality, the concentrations of the elements may vary in the same type of mineral. Moreover, very often one element can substitute another element (either partially or completely) in the same type of mineral.

This section describes the ANN algorithm for quantitative elemental analysis based directly on the intensities of spectral lines obtained by LIBS. The ANN for quantitative assay requires much higher precision than the sample identification. The output neurons now predict the concentrations, which can range from parts per million up to a hundred percents. Thus, to improve the accuracy of the prediction, we introduce the following changes to the structure of a typical ANN and the learning process.

In our earlier development of quantitative analysis of geological samples, the ANN consisted of multiple neurons at the output layer. Each output neuron returned the concentration of one oxide (Motto-Ros et al., 2008). This network, however, can suffer from undesirable cross-talk. During training process, an update of any weights or biases by one output can change the values of other output neurons, which may be optimized already. Therefore, in this current algorithm, we propose using several networks and each network has only one output neuron dedicated to one element's concentration (Fig. 13). For geological materials, we use conventional representation of concentration of element's oxide form.

Similar to identification algorithm in low-signal condition, the spectral lines identified for the same element are averaged producing one input value per element. This minimizes the noise due to individual fluctuation of lines.

Since the concentration of the oxide can cover a wide range, during the back-propagation training, the network unavoidably favour the fitting of high concentration values and cause inaccurate predictions at low concentration elements. To minimize this bias, the input and desired output values are rescaled with their logarithm to reduce the data span and increase the weight of the low-value data during the training.

Without the matrix effect, the concentration of an element can simply be determined by the intensity of its corresponding line by using a calibration curve. In reality, the presence of other elements or oxides introduces non-linearity. To present this concept in an ANN, additional inputs corresponding to other elements are added. Those inputs however should be allowed to play only secondary role as compared to the input from the primary element. In other words, the weights and biases of the primary neurons should weight more than others should.

To implement this idea, the ANN training is split into two steps. In the first training, only the average line intensity of the oxide of interest is fed to the network. This average intensity is duplicated to several input neurons to improve the convergence and accuracy. The weights and biases obtained from this training are carried forward to the second training of
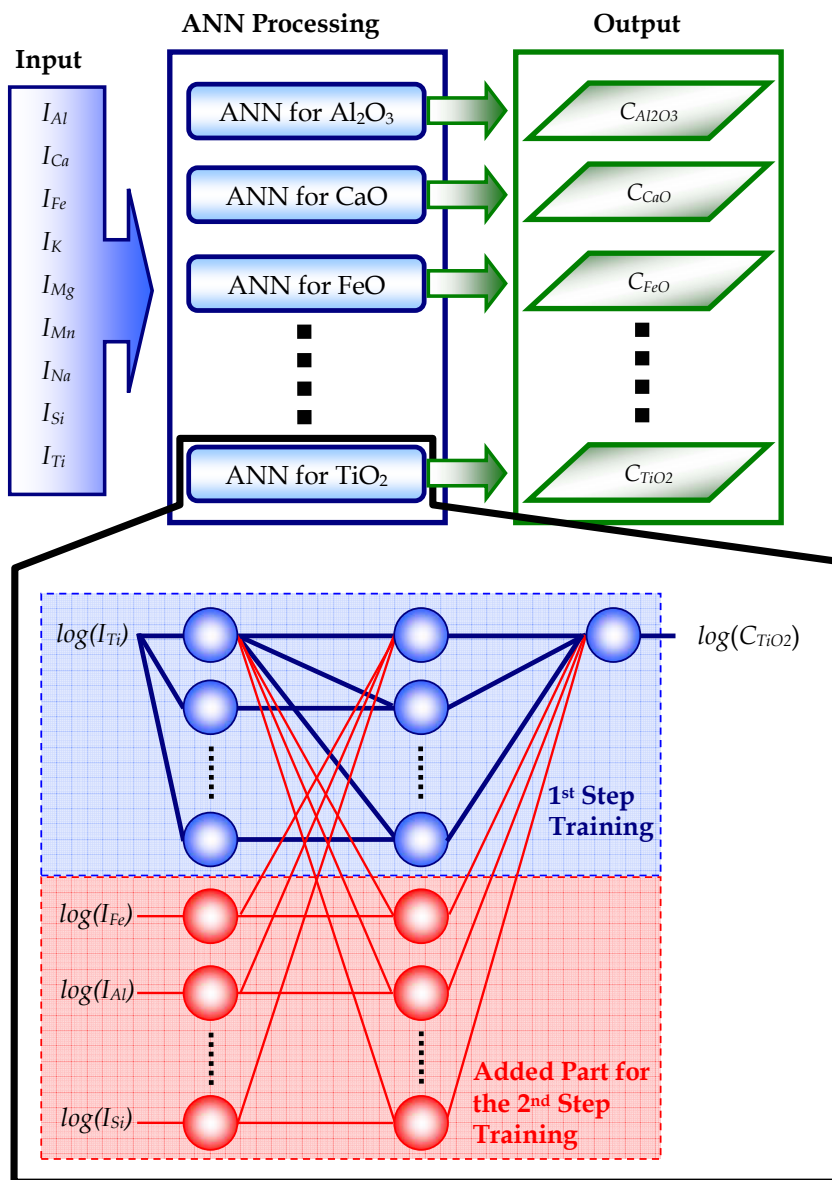
Fig. 13. Architecture of the expanded ANN for the constructive training. The blue dashed box indicates the structure of the ANN corresponding to the 1st step training. The red dashed box shows the neurons and connections added to the initial network (blue) during the 2nd training (constructive). In the 2nd training, the weights and biases of the blue neurons are initialled with the values obtained from the first training, while the weights and biases of the red neurons are initialized with small values much lower than those of blue neurons.
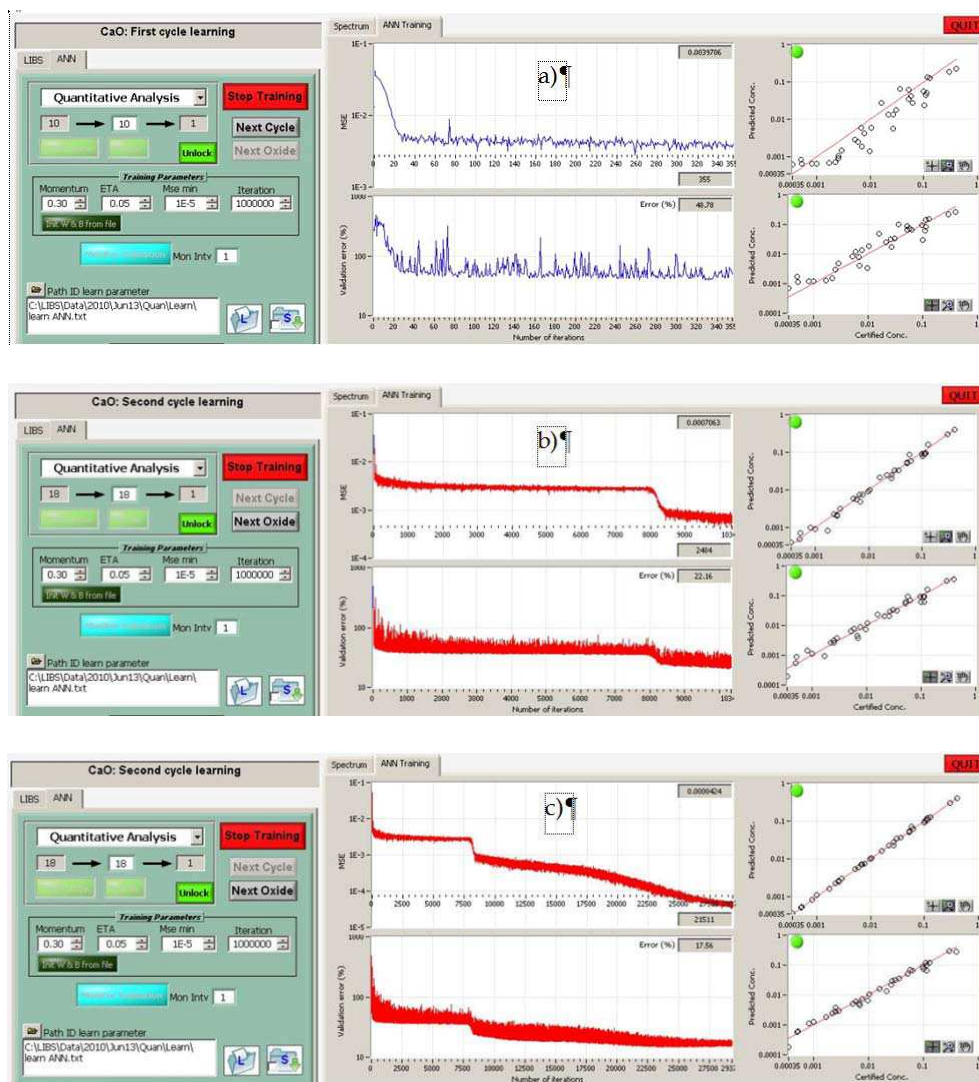
Fig. 14. Screenshots of the training interface of the quantitative LIBS-ANN algorithm programmed in LabView environment. Dynamics of the ANN learning and validation error while training is shown: (a) – during the 1st step training; (b) – in the beginning of the 2nd step training; (c) – at the end of the training. On each screenshot: the menu on the left defines training parameters; the graph in middle-top shows mean square error (MSE) for the training set; the graph in middle-bottom shows MSE for the validation set; the graph in right-top shows predicted concentration *vs.* certified concentration for the training set; the graph in right-bottom shows predicted concentration *vs.* certified concentration for the validation set.

a larger network. The expanded network is constructed from the first network with additional neurons which handle other spectral lines. This two-step training is referred as constructive training. Accuracy is verified by validation data set simultaneously with training (Fig. 14).

This figure illustrates training dynamics on the ANN part responsible for CaO measurement. In the first step of training the ANN has one input value per material that is copied to 10 input neurons. The number of hidden neurons is 10 and there is only one output neuron. As we see, the validation error is very noisy and reaches rather big value at the end of the training (~50%) (Fig. 14a). Concentration plot shows large scattering. When the second training starts the error goes down abruptly. In this case the network is expanded to 18 input neurons (10 for CaO line and 8 for the rest of elements, one input per element). The number of hidden neurons is 18 and there is one output neuron corresponding to CaO concentration. The validation error and the level of noise get gradually reduced. At the end of the training it reaches 17 % (averaged value for the data set). Taking into account that the span of data reaches four orders of magnitude, this is a very good unprecedented performance.

A comparison of the performance between a typical ANN using conventional training and a re-structured ANN with constructive training is shown in (Fig. 15a, b). In general, the predictions by the constructive ANN fall excellently on the ideal line (i.e., predicted output corresponds to certified value). Although the performance is similar at high concentration region (>10%), the data from the conventional ANN method start to deviate at low concentration regime. The scattering of data becomes very large at the very low concentration region (< 0.1%). Some data points fall outside the displayable range of the plot (e.g. the low concentrated TiO_2 and MnO). This observation supports the importance of data rescaling for accurate predictions at low concentration range.

The performance of validation for different oxides is summarized in Table 3. The validation by the constructive method is significantly better than that of the conventional training. The deviation of all predictions is less than 20%. The prediction of SiO_2 concentration is similar in both approaches since it is the most abundant oxide in almost all samples. For the conventional ANN method, the deviations of most prediction are in general higher. This is attributed to the cross-talk of the neurons. The deviation for MnO is incredibly large as it is usually in the form of impurity of tens of ppm. Thus the bias in training makes the prediction of these low concentrated oxides less accurate.

Oxide	Al_2O_3	CaO	FeO	K_2O	MgO	MnO	Na_2O	SiO_2	TiO_2
Constructive ANN error (%)	17.7	14.1	14.3	16.9	14.0	18.9	10.7	7.7	16.6
Conventional ANN error (%)	21.3	33.3	44.2	33.4	53.2	152.5	35.9	7.3	86.6

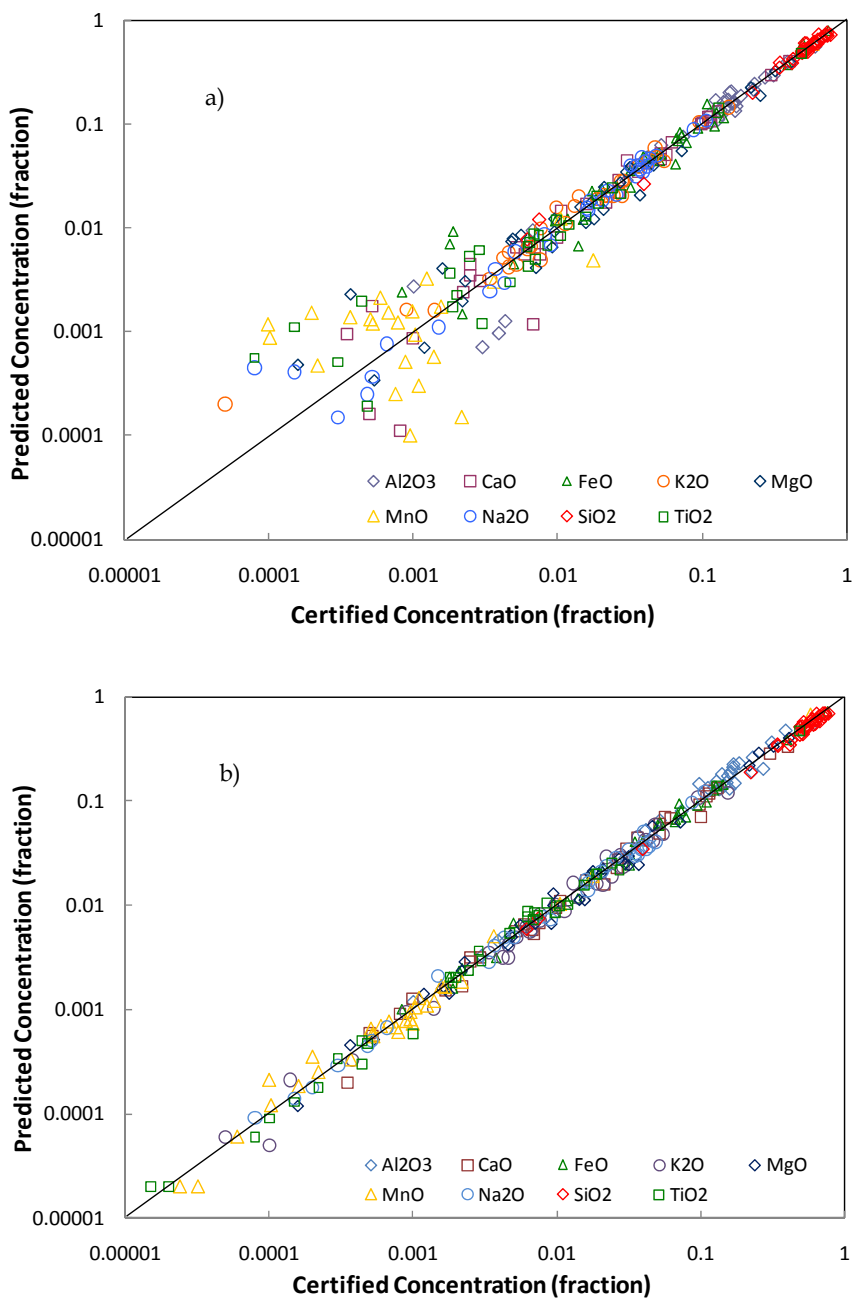Table 3. A comparison of the validation error between the constructive and conventional ANN.

Fig. 15. A comparison of the validation performance between a typical ANN with conventional training (a) and the ANN with constructive training (b).

The prediction of oxide concentration by the constructive ANN is evaluated by four certified samples, which were not part of the training process. They were unknown to network thus simulating a new sample. The oxide concentrations obtained are compared with those calculated using the calibration curve method and a conventional ANN algorithm (Fig. 16). Among these three techniques, both the calibration curve method and the conventional ANN give inaccurate prediction for most oxides (Table 4).

For the calibration curve method, the deviation is mainly due to the serious matrix effects of the geological samples.
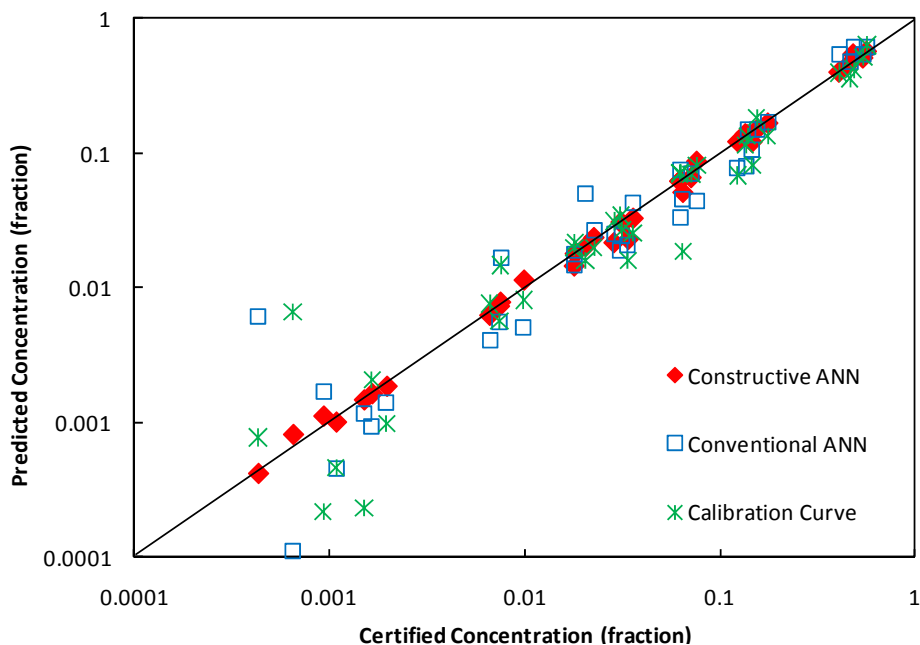
Fig. 16. Comparison of the concentration prediction of the four samples (andesite JA2, basalt BCR2, iron ore, orthoclase gabbro) by the constructive ANN, conventional ANN and the calibration curve method.

The prediction of SiO_2 has the least deviation as it is the major constitution (i.e., the matrix) of the samples. Minor components such as Al_2O_3, CaO, FeO and MgO have errors of about 20 to 30%. Impurities, like MnO, Na_2O and TiO_2, suffer most from the matrix effect and have the worst predictions, which is 40% to 250% inaccuracy.

The conventional ANN has comparable result as that of the calibration curve. Yet their deviation is caused by the limitation of the ANN discussed earlier. The errors for MnO, Na_2O and TiO_2 are still the worst at 50% to over 300% level. For Al_2O_3, CaO and FeO, the variations are around 20%. However, due to cross-talking of the output neutrons, the prediction of SiO_2 is even worse than that obtained from the calibration curve method. Nevertheless, the predictions at low concentration scattered seriously, revealing the bias of high-concentration fitting during the training process.

With the modified ANN, the accuracy of the prediction is drastically enhanced. Those scattered data from the calibration curve method and classical ANN at the low

concentration region are now brought back to the ideal line. Both the major oxides (SiO_2 and Al_2O_3) and the impurities (MnO and Na_2O) have similar performance of deviations below 20%. The matrix effect and the poor accuracy at low concentration that appear in other methods are no longer observed in the optimized constructive ANN technique.

Oxide	Al_2O_3	CaO	FeO	K_2O	MgO	MnO	Na_2O	SiO_2	TiO_2
Constructive ANN deviation (%)	2.8	10.2	0.6	6.0	16.7	8.0	8.1	5.6	10.7
Conventional ANN deviation (%)	18.1	24.1	22.9	47.0	25.3	47.2	71.6	17.8	360.3
Calibration curve deviation (%)	20.3	19.6	20.9	37.6	29.0	67.2	241.3	8.3	40.0

Table 4. The average deviation of the prediction from the certified value for each oxide of the four unknown samples.

Given the success of these two types of analysis demonstrated above: identification and quantitative, we merged them in one software tool to facilitate data analysis (Fig. 17). The identification part uses ANN with 139 input neurons, 140 hidden and 41 output neurons, and the quantitative ANN uses constructive architecture. Two outputs are produced from a single LIBS data acquisition: material identification and its composition prediction. Even if the sample cannot be identified, its composition is still accurately predicted.

4. Conclusion

We demonstrate application of supervised ANN architectures to spectroscopic analysis based on LIBS data. Two distinct processing approaches are described targeting material identification and quantitative material composition analysis.

In the first application, such features as early stopping and sequential training are introduced enabling exceptional robustness of the algorithm. While the algorithm was trained using standard powder-based samples, a 100% successful identification is achieved using set of natural rocks and minerals as test samples. Application of material identification in quantitative mineralogy analysis is demonstrated using artificial mineral mixture. Overall accuracy of 2.5% is achieved.

In the second application, we introduced constructive learning to ensure algorithm stability and robustness, but at the same time to account for matrix effects. The accuracy better than 20% is achieved for nine elements measured in their oxide form (Al_2O_3, CaO, FeO, K_2O, MgO, MnO, Na_2O, SiO_2 and TiO_2) in the working range from 10 parts per million up to a hundred percent. It is worth noting that this accuracy is reached with no assumption on the type of the material. Geological samples of mineralogy different than those used for training the algorithm were successfully tested. This demonstrates the ability of the constructive ANN technique to overcome highly nonlinear multi-dimensional problem caused by matrix effects in LIBS data.
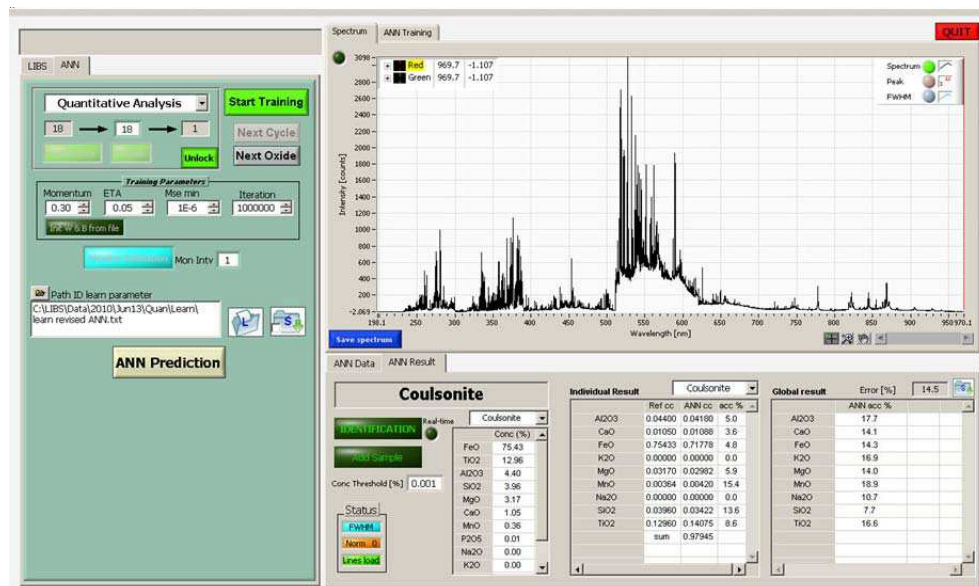
Fig. 17. Measurement of a new sample composition by quantitative ANN-LIBS algorithm implemented in LabView environment complemented by material identification ANN analysis. Upper-left section defines the network parameters and hardware control parameters. Top-right part displays the acquired spectrum. Bottom-right section displays the results of ANN analysis (from left to right): sample identity (Coulsonite in this case) and its tabulated composition, then the sample composition predicted by quantitative ANN, and finally the difference between the predicted composition and the tabulated composition.

Based on the above algorithms, the integrated software tool has been developed. It provides identification, mineralogy, and composition analysis with a single acquisition of LIBS spectra. The future works will be directed toward verification of stability of the algorithms with data acquired in different experimental settings. Use of sequential training for quantitative composition analysis is proposed to enhance this stability. We plan to implement comprehensive validation tests in laboratory and in field conditions.

5. Acknowledgements

6. References

Aguilera, J.A.; Aragón, C.; Cristoforetti, G. & Tognoni, E. (2009) Application of calibration-free laser-induced breakdown spectroscopy to radially resolved spectra from a copper-based alloy laser-induced plasma, *Spectrochimica Acta Part B*, Vol. 64, No. 7, (July 2009) pp. 685-689, ISSN: 05848547

Belkov, M.V.; Burakov, V.S.; De Giacomo, A.; Kiris, V.V.; Raikov, S.N. & Tarasenko, N.V. (2009) Comparison of two laser-induced breakdown spectroscopy techniques for total carbon measurement in soils, *Spectrochimica Acta Part B*, Vol. 64, No. 9, (September 2009) pp. 899-904, ISSN: 05848547

Bousquet, B.; Sirven, J.–B. & Canioni, L. (2007) Towards quantitative laser-induced breakdown spectroscopy analysis of soil samples, *Spectrochimica Acta Part B*, Vol. 62, No. 12, (December 2007) pp. 1582-1589, ISSN: 05848547

Cho, H.H.; Kim, Y.J.; Jo, Y.S.; Kitagawa, K.; Arai, N. & Lee, Y.I. (2001) Application of laser-induced breakdown spectrometry for direct determination of trace elements in starch-based flours, *Journal of Analytical Atomic Spectrometry*, Vol. 16, No. 6, (June 2001) pp. 622-627, ISSN: 02679477

Ciucci, A.; Corsi, M.; Palleschi, V.; Rastelli, S.; Salvetti, A. & Tognoni, E. (1999) New procedure for quantitative elemental analysis by laser-induced plasma spectroscopy, *Applied Spectroscopy*, Vol. 53, No. 8, (August 1999) pp. 960-964, ISSN: 00037028

Clegg, S.M.; Sklute, E.; Dyar, M.D.; Barefield, J.E. & Wien, R.C (2009) Multivariate analysis of remote laser-induced breakdown spectroscopy spectra using partial least squares principal, component analysis, and related techniques, *Spectrochimica Acta Part B*, Vol. 64, No. 1, (January 2009) pp. 79-88, ISSN: 05848547

Cremers, D.A. & Radziemski, L.J. (2006) *Handbook of Laser-Induced Breakdown Spectroscopy*, John Wiley & Sons, ISBN: 978-0-470-09299-6, USA

Eppler, A.S.; Cremers, D.A.; Hickmott, D.D.; Ferris, M.J. & Koskelo, A.C. (1996) Matrix effects in the detection of Pb and Ba in soils using laser-induced breakdown spectroscopy, *Applied Spectroscopy*, Vol. 50, No. 9, (September 1996) pp. 1175-1181, ISSN: 00037028

Escudero-Sanz, I.; Ahlers, B. & Courrèges-Lacoste, G.B. (2008) Optical design of a combined Raman–laser-induced-breakdown-spectroscopy instrument for the European Space Agency ExoMars Mission, *Optical Engineering*, Vol. 47. No. 3, (March 2008) pp. 033001-1 - 033001-11, ISSN: 00913286

Ferreira, E. C.; Milori, D.M.B.P.; Ferreira, E.J.; Da Silva, R.M. & Martin-Neto, L. (2008) Artificial neural network for Cu quantitative determination in soil using a portable laser induced breakdown spectroscopy system, *Spectrochimica Acta Part B*, Vol. 63., No. 10, (October 2008) pp. 1216-1220, ISSN: 05848547

Gaft, M.; Nagli, L.; Fasaki, I.; Kompitsas, M. & Wilsch, G. (2009) Laser-induced breakdown spectroscopy for on-line sulfur analyses of minerals in ambient conditions, *Spectrochimica Acta Part B*, Vol. 64, No. 10, (October 2009) pp. 1098-1104, ISSN: 05848547

Garrelie, F. & Catherinot, A. (1999) Monte Carlo simulation of the laser-induced plasma-plume expansion under vacuum and with a background gas, *Applied Surface Science*, Vol. 138-139, No. 1-4, (January 1999) pp. 97-101, ISSN: 01694332

Gurney K. (1997) *An Introduction to Neural Networks*, UCL Press, ISBN: 0-203-45151-1, UK

Harmon, R.S.; DeLucia, F.C.; McManus, C.E.; McMillan, N.J.; Jenkins, T.F.; Walsh, M.E. & Miziolek, A. (2006) Laser-induced breakdown spectroscopy – An emerging chemical sensor technology for real-time field-portable, geochemical, mineralogical, and environmental applications, *Applied Geochemistry*, Vol. 21, No. 5, (May 2006) pp. 730-747, ISSN: 08832927

Haykin. S. (1999) *Neural Networks: A Comprehensive Foundation*, Prentice Hall, ISBN: 0132733501, US

Iida, Y. (1990) Effects of atmosphere on laser vaporization and excitation processes of solid samples, *Spectrochimica Acta Part B*, Vol. 45, No. 12, (December 1990) pp. 1353-1367, ISSN: 05848547

Inakollu, P.; Philip, T.; Rai, A.K.; Yueh, F.-Y. & Singh, J.P. (2009) A comparative study of laser induced breakdown spectroscopy analysis for element concentrations in aluminum alloy using artificial neural networks and calibration methods, *Spectrochimica Acta Part B*, Vol. 64, No. 1, (January 2009) pp. 99-104, ISSN: 05848547

Kadirkamanathan, V. & Niranjan, M. (1993) A function estimation approach to sequential learning with neural networks, *Neural Computation*, Vol. 5, No. 6, (June 1993) pp. 954-975, ISSN 0899-7667

Koujelev, A.; Motto-Ros, V.; Gratton, D. & Dudelzak, A. (2009) Laser-induced breakdown spectroscopy as geological tool for field planetary analogue research, *Canadian Aeronautics and Space Journal*, Vol. 55, No. 2, (August 2009) pp. 97–106, ISSN: 00082821

Koujelev, A.; Sabsabi, M.; Motto-Ros, V.; Laville, S. & Lui, S.L. (2010) Laser-induced breakdown spectroscopy with artificial neural network processing for material identification, *Planetary and Space Science*, Vol. 58, No. 4, (April 2010) pp. 682-690, ISSN: 00320633

Lanza, N.; Wiens, R.C.; Clegg, S.M.; Ollila, A.M.; Humphries, S.D.; Newsom, H.E.; Barefield, J.E. & ChemCam Team (2010) Calibrating the ChemCam laser-induced breakdown spectroscopy instrument for carbonate minerals on Mars, *Applied Optics*, Vol. 49, No. 13, (May 2010) pp. C211-C217, ISSN: 00036935

Lui, S.L. & Cheung, N.H. (2003) Resonance-enhanced laser-induced plasma spectroscopy: ambient gas effects, *Spectrochimica Acta Part B*, Vol. 58, No. 9, (September 2003) pp. 1613-1623, ISSN: 05848547

Lui, S.L. & Koujelev, A.S. (2011) Accurate identification of geological samples using artificial neural network processing of laser-induced breakdown spectroscopy data, *Journal of Analytical Atomic Spectrometry,* (to be published)

Menut, D.; Descostes, M.; Meier, P.; Radwan, J.; Mauchien, P. & Poinssort, C. (2006) Europium migration in argillaceous rocks: on the use of micro laser-induced breakdown spectroscopy as a microanalysis tool, *Materials Research Society Symposium Proceedings*, Vol. 932, (September 2006) pp. 913-918, ISSN: 02729172

Miziolek, A.W.; Palleschi, V. & Schechter, I. (2006) Laser Induced Breakdown Spectroscopy, Cambridge University Press ISBN-13: 9780521852746, ISBN-10: 0521852749, UK

Mönch, I.; Sattmann, R. & Noll, R. (1997) High speed identification of polymers by laser-induced breakdown spectroscopy, *Proceedings of SPIE,* Vol. 3100, No. 1, (September 1997) pp. 64-74, ISSN: 0277786X

Moody, J.E. (1992) The effective number of parameters: an analysis of generalization and regularization in nonlinear learning systems, In: *Advances in neural information processing systems 4*, Moody, J.E.; Hanson, S.J. & Lippmann, R.P., (Eds.), pp. 847-854, Morgan Kaufmann Publishers, ISSN: 1-55860-222-4, USA

Motto-Ros, V.; Koujelev, A.S.; Osinski, G.R. & Dudelzak, A.E. (2008) Quantitative multi-elemental laser-induced breakdown spectroscopy using artificial neural networks, *Journal of the European Optical Society – Rapid Publications*, Vol. 3, (March 2008) 08011, ISSN: 19902573

Prechelt, L. (1998) Early stopping – but when?, In: *Neural Networks: Tricks of the trade*, Orr, G.B. & Müller, K.-R., (Eds.), pp. 55-69, Springer Verlag, ISBN-10: 3540653112, ISBN-13: 9783540653110, Heidelberg, USA

Rajasekaran, S.; Suresh, D. & Vijayalakshmi Pai, G.A. (2002) Application of sequential learning neural networks to civil engineering modeling problems, *Engineering with Computers*, Vol. 18, No. 2, (August 2002) pp. 138-147, ISSN: 01770667

Rajasekaran, S.; Thiruvenkatasamy, K. & Lee, T.L. (2006) Tidal level forecasting using functional and sequential learning neural networks, *Applied Mathematical Modeling*, Vol. 30, No. 1, (January 2006) pp. 85-103, ISSN: 0307904X

Ramil, A.; López, A.J. & Yáñez A. (2008) Application of artificial neural networks for the rapid classification of archaeological ceramics by means of laser induced breakdown spectroscopy (LIBS), *Applied Physics A*, Vol. 92, No. 1, (January 2008) pp. 197-202, ISSN: 09478396

Samek, O.; Telle, H.H. & Beddows, D.C.S. (2001) Laser-induced breakdown spectroscopy: a tool for real-time, in vitro and in vivo identification of carious teeth, *BMC Oral Health*, Vol. 1, PMC64785, ISSN: 14726831

Sattmann, R.; Mönch, I.; Krause, H.; Noll, R.; Couris, S.; Hatziapostolou, A.; Mavromanolakis, A.; Fotakis, C.; Larrauri, E. & Miguel, R. (1998) Laser-induced breakdown spectroscopy for polymer identification, *Applied Spectroscopy*, Vol. 52 No. 3, (March 1998) pp. 456-461, ISSN: 00037028

Sharma, S.K.; Misra, A.K.; Lucey, P.G.; Wiens, R.C. & Clegg, S.M. (2007) Combined remote LIBS and Raman spectroscopy at 8.6 m of sulfur-containing minerals, and minerals coated with hematite or covered with basaltic dust, *Spectrochimica Acta Part A*, Vol. 68, No. 4, (December 2007) pp. 1036-1045, ISSN: 13861425

Sirven, J.–B.; Bousquet, B.; Canioni, L.; Sarger, L.; Tellier, S.; Potin-Gautier, M. & Hecho, I. Le (2006) Qualitative and quantitative investigation of chromium-polluted soil by laser-induced breakdown spectroscopy combined with neural networks analysis, *Analytical and Bioanalytical Chemistry*, Vol. 385, No. 2, (May 2006) pp. 256-262, ISSN:16182642

Sirven, J.-B.; Sallé, B.; Mauchien, P.; Lacour, J.-L.; Maurice, S. & Manhès, G. (2007) Feasibility study of rock identification at the surface of Mars by remote laser-induced breakdown spectroscopy and three chemometric methods, *Journal of Analytical Atomic Spectrometry*, Vol. 22, No. 12, (December 2007) pp. 1471-1480, ISSN: 02679447

St-Onge, L.; Kwong, E.; Sabsabi, M. & Vadas, E.B. (2002). Quantitative analysis of pharmaceutical products by laser-induced breakdown spectroscopy. *Spectrochimica Acta Part B*, Vol. 57, No. 7, (July 2002) pp. 1131-1140, ISSN: 05848547
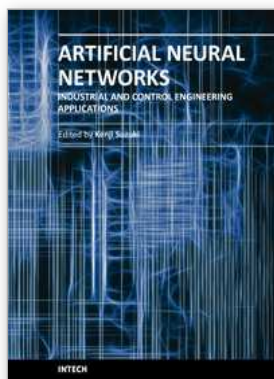
Artificial Neural Networks - Industrial and Control Engineering Applications

Edited by Prof. Kenji Suzuki

Artificial neural networks may probably be the single most successful technology in the last two decades which has been widely used in a large variety of applications. The purpose of this book is to provide recent advances of artificial neural networks in industrial and control engineering applications. The book begins with a review of applications of artificial neural networks in textile industries. Particular applications in textile industries follow. Parts continue with applications in materials science and industry such as material identification, and estimation of material property and state, food industry such as meat, electric and power industry such as batteries and power systems, mechanical engineering such as engines and machines, and control and robotic engineering such as system control and identification, fault diagnosis systems, and robot manipulation. Thus, this book will be a fundamental source of recent advances and applications of artificial neural networks in industrial and control engineering areas. The target audience includes professors and students in engineering schools, and researchers and engineers in industries.

How to reference

In order to correctly reference this scholarly work, feel free to copy and paste the following:

Alexander Koujelev and Siu-Lung Lui (2011). Artificial Neural Networks for Material Identification, Mineralogy and Analytical Geochemistry Based on Laser-Induced Breakdown Spectroscopy, Artificial Neural Networks - Industrial and Control Engineering Applications, Prof. Kenji Suzuki (Ed.), ISBN: 978-953-307-220-3, InTech, Available from: http://www.intechopen.com/books/artificial-neural-networks-industrial-and-control-engineering-applications/artificial-neural-networks-for-material-identification-mineralogy-and-analytical-geochemistry-based-

INTECH
open science | open minds